INSTITUTE OF PLASMA PHYSICS

NAGOYA UNIVERSITY

RESEARCH REPORT

NAGOYA, JAPAN

PLASMA TURBULENCE GENERATED BY ION-ION TWO-STREAM INSTABILITY

Y. Kiwamoto* and H. Ikezi

IPPJ-184 February 1974

Further communication about this report is to be sent to the Research Information Center, Institute of Plasma Physics, Nagoya University, Nagoya, JAPAN.

---

* Present Address: Institute of Materials Science and Engineering, Yokohama National University, Yokohama, 233.

Abstract

Strong instability is produced by injecting a high density ion beam with a large cross-section into an unmagnetized homogeneous plasma. The linear dispersion relation of the waves in the ion-ion two-stream system is experimentally confirmed. Three-dimensional investigations of the turbulence thus produced reveal some new features: The turbulent waves propagate at large angles to the beam with extremely short correlation length of (2-3)·wavelength. At these angles a rapid relaxation of the velocity distribution of the ions is observed until the beam temperature reaches around $T_e/5$. The energy density of the turbulence does not exceed $3 \times 10^{-3}\ n_p T_e$.

§1. Introduction

In the long history of the studies of the beam-plasma interactions[1-5], the experiments on the ion beam-plasma interaction have been initiated only in recent years. The instabilities, generated by the injection of an ion-beam into a plasma, are interested both from the point of view of understanding of the involved processes and from that of the application to the heating of a fusion plasma. The first experiment on this problem was made by Borisenko and Kirichenko[6]. By injecting a potassium ion beam into an unmagnetized argon plasma, they have observed ion-acoustic density perturbations with broad frequency spectra accompanying a rapid plateau formation in the velocity distribution function of the ions. The collective oscillations are due to the two-stream instability between the two groups of ions (i-i instability)[2,5]. Further investigations were carried out by Baker in the Q-machine[7,8]. He has studied on the linear stability of the ion beam-plasma system and on the evolution of an ion-acoustic turbulence. The investigations of the linear stability have shown that the i-i system is stabilized when the beam velocity is decreased to ion thermal velocity. Taking notice on this feature he has remarked that the saturation of the spatial growth of the turbulence is due to a quasilinear change of the velocity distribution of the ions into a stable form.

As will be discussed later, the i-i instability occurs

in a oblique direction to the beam. The two experiments referred to above were carried out in a plasma with a small cross-section. In order to eliminate geometrical effects especially in the transverse direction, a large uniform plasma is required. Strong i-i instability can be produced in the large unmagnetized plasma[10] in which the effects due to the plasma boundary are utterly negligible. Recently Taylor and Coronitti[9] have studied the turbulence generated by the i-i instability using the same type of plasma. By observing the spatial evolution of the distribution of the parallel component of the ions (the parallel velocity distribution), they have found that the effective parallel temperature increases exponentially until it reaches about one-fifth of the electron temperature T_e. They have noticed also that the rapidly growing electron density fluctuation $\delta n/n_0$ saturates at a relatively low level of 5×10^{-2}. They have concluded that the waves stop growing because the modification of the ion orbits due to random accelerations destroys their coherence; this conclusion is quite different form that of Baker. However, above reports have restricted their investigations to one-dimensional observations.

Before concerning sophisticated discussions on the saturation mechanism of the turbulence, we find the importance of the fact that the evolution of the turbulent waves and their interaction with the ions take place in a three-dimensional way. The purpose of this paper is to explore

the three-dimensional nature of the beam-plasma system[16] and of the structure of the turbulence.

For this purpose the projected ion velocity distribution $f(v, \theta)$ to a plane which makes an angle θ with the beam is observed. This observation enables the correspondence between the propagation of the turbulent waves and the dynamics of the ions. The propagations of the turbulent waves are studied by the use of the spatial correlation technique. An investigation employing these techniques elucidates that the distribution of the beam ions $f_b(v, \theta)$ is dragged strongly in the direction the most unstable wave propagates. It is also revealed that the correlation lengths of the turbulent waves are extremely short in their directions of propagation. Experiments were carried out firstly to examine the characteristics of the linear dispersion relation and marginal stability conditions of the system and then to investigate comprehensively the turbulence thus produced.

In a remaining part of this section the linear dispersion relation of the ion beam-plasma system is briefly described. In §2 experimental apparatus and methods are described. Detailed descriptions of experimental results are made in §3. Section 4 is devoted to discussions, and conclusions of the present experiments are summarized in §5.

The linear dispersion relation of an ion beam-plasma system[5] is

$$1 + \frac{k_D^2}{k^2} - \frac{\omega_{pi}^2}{k^2}\left\{\left(1 - \frac{n_b}{n_p}\right)\int dv\ \frac{k\frac{\partial}{\partial v} f_i(v,\theta)}{kv - \omega}\right.$$

$$\left. + \frac{n_b}{n_p}\int dv\ \frac{k\frac{\partial}{\partial v} f_b(v,\theta)}{kv - (\omega - ku\cdot\cos\theta)}\right\} = 0. \qquad (1)$$

Here, the three-dimensional dispersion relation is reduced to one-dimensional form by projecting vectors such as $\vec{v}$ and $\vec{u}$ (the drift velocity of the ion beam) to the wave-number $\vec{k}$ which makes an angle $\vec{\theta}$ with $\vec{u}$. Electrons are assumed to form a massless fluid and their contributions are represented by k_D^2/k^2, where k_D is the electron Debye wave-number $1/\lambda_D = (4\pi n_p e^2/T_e)^{1/2}$. The contribution of the beam ions with density n_b is written in the beam frame. The distribution function $f_i(v, \theta)$ represents the background ions in the target plasma. If both the temperatures of the background ions $T_i(\theta)$ and of the beam ions $T_b(\theta)$ are sufficiently small compared to the kinetic energy $m_i u^2/2$ of the beam ions, eq.(1) is reduced to a fourth-order algebraic equation for angular frequency ω, and one of the branches belongs to a negative energy wave[4]. When $n_b/n_p \sim 1$, this beam mode is unstable, if $|u\cdot\cos\theta| < 2c_s$, through the coupling with an ion-acoustic mode which belongs to the background ions. Here, c_s is the ion acoustic velocity $(T_e/m_i)^{1/2}$. It should be noted that the unstable waves can propagate at finite angles to the beam even if

$u/c_s < 2c_s$. As u increases, a stable corn in the wavenumber space sets in; the angle θ_c of the corn increases with u. In the present experiment this feature was clearly observed; this fact evidently points out the necessity of three= dimensional investigations of the turbulence.

§2. Experimental Methods

The experiment has been carried out in the Double Plasma Device (DP ~ Machine) which is schematically shown in Fig.1. The detailed description of this machine has been made in refs. 10 and 11. This device consists of two electrically insulated plasmas, the driver plasma and the target palsma, both having dimensions of 40 cm in diam. and 40 cm in length. The ions in the driver plasma are stationarily injected into the target plasma through the potential difference V_b imposed between the two plasmas, and form a large diameter homogeneous ion beam with a density n_b which is variable from 10^7 cm^{-3} to 10^9 cm^{-3}. The kinetic energy of the beam ions $m_i u^2/2$ is equal to eV_b which can be varied up to 30 eV. Argon gas with pressure $p = (1 - 4) \times 10^{-4}$ Torr is used. The charge exchange mean-free-path of the beam ions is typically 15 cm[14]. Plasma density, $n_p = n_i + n_b$, can be varied from 4×10^8 cm^{-3} to 2×10^9 cm^{-3}. Electron temperature T_e ranging from 1 to 4 eV in normal operation can be lowered down to 0.5 eV by the following method:

When the chamber wall is covered by a semiconductor layer, which consists of evaporated filament material and the vapor of pump oil, the plasma potential is somewhat lower than that of the wall and the electron temperature is typically 3 eV. A large clean mesh grid is placed near the anode wall on the opposite side to the driver plasma. By increasing the potential applied to the mesh grid relative to the wall, the high energy components of the electrons are absorbed by the mesh grid, and the lower electron temperature results.

An electrostatic ion energy analyzer shows that the temperature of the background ions T_i is 0.1 - 0.2 eV. It also reveals that the energy half-width of the velocity distribution function of the beam ions $f_b(v, \theta = 0^\circ)$ remains unchanged regardless of the value of eV_b, unless they are heated by the turbulence. This observation indicates that the parallel beam temperature $T_{b\parallel}$ is effectively decreased from the temperature T_i (the value when the ions are not accelerated) down to $T_i^2/4\ eV_b$. Because the transverse beam temperature $T_{b\perp}$ is not affected by the acceleration, the velocity distribution of the beam ions $f_b(v, \theta)$ is strongly anisotropic. In order to observe the evolution of $f_b(v, \theta)$, a rotatable energy analyzer with a window of 2 cm in diam. is used. The surface of the metal container of the energy analyzer is coated with an insulator layer so that the plasma disturbance due to the analyzer is minimized. The energy resolving power of the analyzer is

0.1 eV in the beam direction. The relatively large window dimension of the analyzer loses spatial resolution so that we observe averaged $f_b(v, \theta)$ over the dimension of the analyzer.

In order to investigate the evolution of the turbulent waves the spatial correlation technique is employed. The plasma density fluctuations $\delta n/n_0$ are detected by two separate plane probes (2 mm × 2 mm each) biased slightly above the plasma potential. As is shown in Fig.1, one probe is moved along the beam direction, and the other transversely to it. The two signals are fed into a balanced mixer through tuned amplifiers with the Q-value of 20. Taking a time average of its output we obtain a spatial correlation of the density fluctuations. The spatial correlation parallel to the beam shows the parallel wavelength $2\pi/k_{\parallel}$, and the one transverse to the beam shows the transverse wavelength $2\pi/k_{\perp}$. Combining the two wavelengths, $2\pi/k_{\parallel}$ and $2\pi/k_{\perp}$, we can determine the propagation direction of the wave, its wavelength $2\pi/k$, and correlation length L_c in the direction of its propagation.

§3. Experimental Results

3.1 Propagation of test wave

We first examine the characteristics of the linear dispersion relation of the waves in the ion beam-plasma system. Test waves are launched from a large plane mesh grid which separates the two plasmas. The grid launches the waves in the direction of the ion beam. Since the dispersion relation given by eq.(1) has several branches, the waves with different phase velocities are excited simultaneously. In order to separate each wave, we employ the time-of-flight method of a pulsed test wave. Sampling technique is employed in order to separate the test waves from spontaneously excited turbulent waves.

When the beam velocity u is small compared with $2c_s$, two waves are excited. Figure 2 shows a typical wave response. The beam velocity u/c_s is 1.25 and the density fraction of the beam ion n_b/n_p is 0.5. Although the fast wave damps away monotonically, the slow wave grows rapidly and saturates around $x = 40\ \lambda_D$. From Fig.2 the phase velocities of the two waves ω/kc_s are estimated to be 1.52 and 0.77 respectively. The growth rate k_i of the slow wave is estimated to be about $0.04\ k_D$ in the early stage of its growth. The representative frequency ω of the slow wave at $x = 2$ cm and 3 cm is $2\pi \times 10^5$ rad/sec $\simeq 0.14\ \omega_{pi}$. The real part of the wavenumber is found to be $k_r \simeq 0.2\ k_D$, so that we have a very large growth rate $k_i \simeq 0.2\ k_r$.

This fact clearly indicates the non-resonant nature of the i-i instability. When u is increased to a value above $2c_s$, the slow wave is observed to be stable and we find a third wave which has a phase velocity of about c_s.

By examining the propagations of the test waves for different values of u/c_s, we obtain the dispersion relation shown in Fig.3. The dots represent the experimental results when T_e = 3 eV and n_b/n_p = 0.2. Here, we followed the position of the peak of each wave pulse. Strictly speaking, the velocity thus obtained is not a true phase velocity. However, because of very weak dispersion of the wave the difference of the measured velocity from the true phase velocity is small. The data points reduced from Fig.2 are also indicated by circles (real parts) and a triangle (growth rate of the slow wave). It is noted taht c_s is $(T_e/m_i)^{1/2}$ and is not the experimentally observed ion= acoustic velocity. When $u/c_s = 0$, the phase velocity of the fast wave is slightly larger than c_s; this is due to the finite ion temperature, and is consistent with the experimental condition of $T_e/T_i \approx 20$. The theoretically predicted phase velocities, which are calculated from eq.(1) in the limit of long wavelength, are shown by solid lines. The imaginary part of ω/kc_s for the unstable slow wave is shown by the dotted line. In the calculation, the distributions $f_i(v, \theta)$ and $f_b(v, \theta)$ are assumed to be Maxwellian, and the typical experimental parameters, $n_b/n_p = 0.2$, $T_e/T_i = 20$ are used. The cooling of the beam

ions by the acceleration is taken into account by the use of the approximate equation

$$T_{b//} = \frac{T_i^2}{2m_i u^2 + T_i} \cdot \qquad (2)$$

Although even a hydrodynamic approximation can give a fairly satisfactory dispersion relation as long as its real part is concerned, the imaginary part is affected by the finite temperature of the ions especially around the marginally stable region of u. By examining the spatial evolutions of the test waves, the marginal states which divide the stable and the unstable regions in $m_i u^2/2T_e - T_e$ plane are found, and are shown by dots in Fig.4. The bars indicate the ambiguities in the measurement. The marginal states labelled by A and B are found. The points on family A are obtained when $T_e \gtrsim 0.8$ eV, and those on B result when T_e is below 0.8 eV. When $T_e \lesssim 0.8$ eV, spontaneously excited density fluctuation $\delta n/n_0$ is reduced below 10^{-2}. Theoretical curves of the marginal states are calculated from eqs.(1) and (2) for both Maxwellian distribution and Lorentzian distribution[5], and are shown in Fig.4. The temperature of the Lorentzian distribution is defined by the velocity half-width. The calculation with Maxwellian distribution functions does not give upper limit of $m_i u^2/2T_e$ for the instability. On the other hand Lorentzian distribution functions give marginal states which fit the experimental results. The peculiar feature of the marginal

states for the Maxwellian is due to the very weak contribution of resonant ions. Indeed, we have found a very small growth rate of the slow wave mode when $u/c_s > 2$. This growth rate decreases exponentially with u/c_s, so that the instability can be easily stabilized by the introduction of very weak collisions. In this sense, the plausible agreement of the Loretzian distribution with the experimental results does not necessarily assure its superiority over the Maxwellian distribution. The long tail of the Lorentzian distribution has an effect equivalent to the collisional stabilization of the i-i instability. This feature will be considered in a later section in connection with the saturation of the turbulence. The origin of family B is not known yet. The discussions hereafter are confined to the case of $T_e > 1$ eV. In the above investigations, it has been confirmed that we are dealing with a non-resonant i-i instability.

3.2 Evolution of turbulent noise

When no test wave is launched, a turbulent noise which has a broad frequency spectrum grows. The feature of the turbulence depends on the plasma parameters such as u/c_s and n_b/n_p. Its dependence on n_b/n_p is rather weak; the fractional density perturbation $\delta n/n_0$ is maximized when $n_b/n_p = 0.5$, and decreases by a factor of 2 when $n_b/n_p = 0.1$[9]. Hereafter the consideration will be confined to the case when $0.2 \leq n_b/n_p \leq 0.5$.

We first study how the evolution of the noise level $\delta n/n_0$ changes when the beam velocity u is increased from zero to a large value. Figure 5(a) shows $\delta n/n_0$ at different positions x as a function of the kinetic energy of the beam $m_i u^2/2$. Here, $m_i u^2/2$ is changed by continuously increasing the potential difference V_b between the two plasmas with parameters other than n_b/n_p kept constant. When V_b is changed in this way, the ion current from the driver plasma is constant when $eV_b \gtrsim T_e$; therefore n_b decreases like $V_b^{-1/2}$. In the case of Fig.5(a), n_b/n_p is 0.3 (when $m_i u^2/2 < 2$ eV) and $0.3 \cdot (4/m_i u^2)^{1/2}$ (when $m_i u^2/2 \geq 2$ eV). Because of the charge exchange process n_b/n_p decreases as x is increased. Above values are obtained at x = 5 cm. The evolution of $\delta n/n_0$ in the case of $m_i u^2/2 \lesssim 2T_e$ is different from that in the case of $m_i u^2/2 \gtrsim 2T_e$. When the beam energy is small, the fluctuation grows rapidly and soon damps after the saturation. In contrast, when $m_i u^2/2 > 2T_e$, $\delta n/n_0$ does not level off soon, but continues growing with a much smaller growth rate. In any case the eventual saturation level of $\delta n/n_0$ is insensitive to $m_i u^2/2$. The spatial evolution of $\delta n/n_0$ is more clearly shown in Fig.5(b). The initial growth rate becomes smaller as $m_i u^2/2$ increases. When $m_i u^2/2 \gtrsim 2T_e$, $\delta n/n_0$ grows not simply exponentially but rather in an oscillatory manner. This fact suggests that there is a preferential growth of a particular group of waves at each stage of the turbulence.

Figure 6 shows the frequency spectra; Fig.6(a) repre-

sents the case of $u/c_s < 2$, and Fig.6(b) that of $u/c_s > 2$. The i-i instability generates a noise which has a broad frequency spectrum ranging from 0 up to f_{pi}. A clear difference is observed between the two cases. When $u/c_s < 2$, all of the waves grow very quikly and saturate almost at the same position. When $u/c_s > 2$, however, the waves with frequency $f \approx f_{pi}/2$ firstly start growing. As they level off the lower frequency waves grow. This frequency dependent growth introduces the oscillatory growth of the total amplitude of the fluctuation shown in Fig.5(b). Finally we note that the fluctuation amplitude saturates at rather low level $\delta n/n_0 \approx 6 \times 10^{-2}$ for any value of u/c_s. The energy density of the fluctuating electric field

$$\sum_{\vec{k}} \frac{\partial}{\partial \omega_{\vec{k}}} [\omega_{\vec{k}}(\vec{k}, \omega_{\vec{k}})] \cdot \frac{1}{8\pi} |\vec{E}_{\vec{k}}|^2$$

$$\approx \frac{1}{2} n_p T_e \left(\frac{\delta n}{n_0}\right)^2, \qquad (3)$$

does not exceed $3 \times 10^{-3}\ n_p T_e$.

3.3 Propagation of turbulent waves

Basic features of the turbulent waves such as the direction of the wave propagation, the wavenumber, and the spatial correlation of each component of the waves which constitute the turbulence are investigated. We observe spatial correlation functions of the waves by using two probes. A reference signal of density perturbation is

received at (x, y) = (2.5 cm, 0 cm) where the most unstable waves begins to level off. Here, we take x axis along the beam, y axis transversely to it, and the origin is at the center of the large mesh grid which separates the two plasmas. The parallel correlation functions are obtained in a region between x = 2.5 cm and x = 7.5 cm, and the perpendicular one between y = 0 cm and y = 5 cm.

Typical examples are shown in Fig.7(a) and (b); each of which corresponds to the case when u/c_s is large ($u/c_s = 2.9$) and that when it is small ($u/c_s = 1$). The parallel spatial correlation functions are indicated by $\parallel$ and the perpendicular ones by $\perp$. Figure 7(a) shows the propagation of the most unstable wave with frequency $f = 0.4\ f_{pi}$. Note the extremely short correlation length in the perpendicular direction. This is not due to the finite frequency band-width of the tuned amplifires. Although the probe dimensions are 2 mm × 2 mm, the spatial resolution of the probes still seems tolerable. Combining the two traces (parallel and perpendicular), we find that the wave propagates to the direction at about 70° off the beam direction with the correlation length $L_c \gtrsim 2\lambda \gtrsim 50\lambda_D$ and with the wavelength $\lambda \gtrsim 25\lambda_D$. As is seen in Fig.4 this is the case when the waves propagating in the beam directions are stable. The large angle between the wavenumber and the beam clearly reveals the three-dimensional nature of the instability.

It is interesting that even in the case when the system

is unstable in the beam direction, high frequency components of the noise propagate at large angles to the beam. Figure 7(b) shows the correlation functions of a relatively high frequency component ($f = 0.3\ f_{pi}$) in the case when $u/c_s = 1.0$. This wave propagates at about 40° to the beam with a relatively long correlation length $L_c \approx 4\lambda$. It is observed taht the dominant part of the waves propagate at angles ranging from 0° up to 30°.

The following findings have been obtained from the measurements of the correlation functions:

(a) The angle θ^* between the wavenumber of the most unstable wave and the beam increases with u/c_s. In Fig.8 the observed angles of the dominant waves are plotted as a function of u/c_s. The solid line represents the angle θ^* [$= \cos^{-1}(1.2\ c_s/u)$] of the most unstable wave which is estimated from the cold ion two-stream model.

(b) The critical angle θ_c for the instability increases with u/c_s. The shaded region in Fig.8 indicates the stable directions expected from the stability condition $u \cdot \cos\theta > 2c_s$.

(c) The dispersion relation $\vec{k} = \vec{k}(f)$ of the unstable wave is known from the correlation functions. For given u/c_s, both the amplitude and the angle of $\vec{k}$ increase with the frequency.

(d) The phase velocities lie in a range from $0.6\ c_s$ to c_s; this is consistent with the dispersion relation shown in Fig.3. For given u/c_s, the width $\Delta(\omega/k)$ of the distribution of the phase velocities is about $0.2\ c_s$.

(e) In contrast to the parallel correlation length, the transverse correlation length is very short; it is less than $50\lambda_D$. The representative correlation length in the direction of the wave is $L_c = (2 - 3)\lambda$.

3.4 Evolution of ion distribution

As the turbulence grows the fluctuating electric fields accelerate ions randomly, and consequently the distribution of the ions is deformed. It has been found that the turbulent waves propagate at large angles to the beam and they are heavily damped in those directions. This fact implies that $f(v, \theta)$ is strongly deformed for large θ and consequently the growth rates of the waves are reduced. By the use of the energy analyzer, the evolution of $f(v, \theta)$ [= $f_i(v,\theta) + f_b(v,\theta)$] is observed as a function of angle θ. Figure 9 shows typical results of the measurements for $u/c_s = 1.8$ (Fig.9(a)-(c) and $u/c_s = 1.2$ (Fig.9(d)). Here, the spatial evolution of $f(v, \theta)$ for each direction is shown as a function of the ion energy. The distribution function consists of two peaks. The peaks at the left represent $f_i(v, \theta)$, and those at the right $f_b(v, \theta)$. The scale of the abscissa is 2 eV/div., and the position of the peak of $f_i(v, \theta)$ indicates the plasma potential. When u/c_s is large, as is shown in Fig.9(a), $f(v, \theta = 0^\circ)$ keeps its two-stream shape even after the turbulent noise levels off. On the contrary the ions are filled rapidly in the depression of $f(v, \theta = 0^\circ)$, and eventually a plateau is formed

when u/c_s is small (Fig.9(d))[18,19]. It should be noted, however, that the turbulent noise saturates prior to the formation of the plateau even in the latter case. The formation of a plateau is also observed at large angles to the beam when u/c_s is large. Two examples, $f(v, \theta = 20^\circ)$ and $f(v, \theta = 46^\circ)$, are shown in Fig.9(b) and Fig.9(c). As θ increases, the relaxation of $f(v, \theta)$ becomes more rapid. Here, we note that the beam ions initially have a strong anisotropy which is seen in Fig.9(a)-(c). The initial anisotoropy makes the heating of the ions for large θ less obvious. However, the rapid disappearance of two-stream shape in $f(v, \theta)$ for large θ should be noted. As u/c_s increases, the position where the two-stream shape disappears moves far away from the beam injection point.

Let us estimate the relaxation rates of $f_b(v, \theta)$. Because of the charge exchange process, the ion beam density n_b decreases for larger x. From Fig.8(a) the attenuation length of n_b is estimated to be about 13 cm which is equal to the charge exchange mean-free-path of the argon ion with energy 5 eV[14]. As it is difficult to experimentally separate the beam ions from the background ions, we assume, for convenience, that a part of $f(v, \theta)$ which lies in the region of $m_i v^2/2 \geq 0.6$ eV belongs to the beam component. The attenuation of the mean kinetic energy of the beam ions $m_i u^2/2$ and the change of the effective temperature $T_b(\theta)$ are shown in Fig.9(e). The parallel temperature $T_b(\theta = 0^\circ)$ ($\equiv T_{b\parallel}$) increases exponentially with an e-folding heating

length $\ell_{//} = 30\lambda_D$ and reaches the value slightly above 0.1 eV. The oblique temperatures $T_b(\theta = 20^\circ)$ and $T_b(\theta = 46^\circ)$ increase with the heating length of $\ell = 360\lambda_D$. Extrapolations of $f_b(v, \theta)$ to the range below o.6 eV suggest that $T_b(\theta)$ does not exceed 0.6 eV = $T_e/5$. The fact that the heating rates of $T_b(\theta = 20^\circ)$ equals that of $T_b(\theta = 46^\circ)$ suggests that $T_b(\theta = 90^\circ)(\equiv T_{b\perp})$ increases with the e-folding length of $\ell = 360\lambda_D$. The attenuation length of $m_i u^2/2$ is estimated to be $550\lambda_D$.

§4. Discussion

4.1 Saturation of turbulent waves

We discuss the mechanism of the saturation of the turbulent waves. It has been observed that a turbulent noise saturates at a relatively low level $(\delta n/n_0)^2 \approx 3 \times 10^{-3}$ and that the dominant waves propagate at large angles to the beam with very short correlation length.

4.1.1 Deformation of $f(v, \theta)$

The rapid relaxation of $f_b(v, \theta)$ shown in Fig.9 suggests that the non-resonant i-i instability is stabilized by the filling of the depression of $f(v, \theta)$. A discussion based on the water-bag model is illuminating[17]. Let us consider a rectangular ion distribution with width a and height 1/4a for $f_i(v, \theta)$ and $f_b(v, \theta)$ as is shown in

Fig.10(a). From a simple calculation, it can be shown that the increase of the width a does not stabilize the most unstable wave. Then let us add the third group of ions which correspond to those filling the depression in the distribution; the distribution function is then like one shown in Fig.10(b). The density of the third group of ions is assumed to be n_3. From a simple calculation it is found that the new i-i system is stabilized when

$$n_3 \geq \frac{2n_b\left[1 - \left(\frac{u\cdot\cos\theta}{2c_s}\right)^2\right]}{1 + \left(\frac{u\cdot\cos\theta}{2c_s}\right)^2} \approx 0.5n_b \qquad (4)$$

is satisfied. This stabilization of the instability is due to the fact that the third group of ions shield the space charge brought forth through the interaction of two other streams. We rewrite (4) in terms of the heights of the distribution function, η_b, η_i and η_3, in the form

$$\eta_3 \geq 0.5\eta_b. \qquad (5)$$

Here, we have assumed $\eta_b = \eta_i$. If we approximate the observed distribution by the water-bag and use the criterion (5), the instability is predicted to stop at x = 6 cm and 3 cm in the direction of $\theta = 20^\circ$ and 46°, respectively, in the case shown in Fig.9. This prediction is consistent with the results of the measurement of the wave amplitude.

Now the problem left to be solved is to know how the

depression in the distribution is filled. The spatial evolution of f(v, x) is described by the diffusion equation[18-20]

$$\frac{\vec{u}}{2} - \frac{\partial f(\vec{v},\vec{x})}{\partial \vec{x}} = \frac{\partial}{\partial \vec{v}} \cdot \overleftrightarrow{D} \cdot \frac{\partial}{\partial \vec{v}} f(\vec{v},\vec{x}), \tag{6}$$

where $\overleftrightarrow{D}$ is a diffusion tensor, which is expressed in different ways depending on the fluctuation level $\delta n/n_0$. When $\delta n/n_0$ is small so that the orbits of the ions can be assumed to be straight, the quasilinear theory can be applied and the diffusion tensor is written as[15,18,19]

$$\overleftrightarrow{D} = \left(\frac{e}{m_i}\right)^2 \sum_{\vec{k}} \frac{\hat{k}\,\hat{k}\,\gamma_{\vec{k}}}{(\vec{k}\cdot\vec{v})^2 + \gamma_{\vec{k}}^2} |\vec{E}_{\vec{k}}|^2, \tag{7}$$

$$\approx \frac{1}{4} \frac{c_s^4}{v^2} u \frac{d}{dx} \left(\frac{\delta n}{n_0}\right)^2 \hat{q}\,\hat{q}, \tag{7'}$$

where $\hat{k} = \vec{k}/k$, $\hat{q} = \vec{q}/q$, and $\vec{q}$ is the wavenumber of the most unstable wave. On the other hand, when $\delta n/n_0$ is large, the orbits of the ions are modified by the waves[20,21]; this effect, in turn, modifies the interaction time between the ions and the waves. Dupree has proposed that the diffusion tensor is described in the form[20]

$$\overleftrightarrow{D} = \left(\frac{e}{m_i}\right)^2 \int_0^\infty dt \sum_{\vec{k}} \hat{k}\,\hat{k} |\vec{E}_{\vec{k}}|^2 \cdot \exp\left[i(\vec{k}\cdot\vec{v} - \omega_{\vec{k}})t - \frac{1}{3}(\vec{k}\cdot\hat{q})^2 D t^3\right] \tag{8}$$

$$\approx \hat{q}\, D\, \hat{q}\ .$$

If $\delta n/n_0$ is so large that the inequality

$$w \equiv \frac{[\frac{D(\hat{q}\cdot\vec{k})^2}{3}]^{1/3}}{k} >> \Delta(\frac{\omega}{k}) \tag{9}$$

holds, eq.(8) is written in the form

$$\hat{q}\ D\ \hat{q} \approx \frac{3}{4}\ q\cdot c_s^3(\frac{\delta n}{n_0})^{3/2}\hat{q}\ \hat{q}. \tag{8'}$$

Combining (6) and (7') or (6) and (8'), we can calculate $f(v, \theta)$. If we assume the initial velocity distribution to be Maxwellian, the saturation levels of $\delta n/n_0$ predicted by (7') and (8') are 0.25 and 2.3×10^{-2}, respectively; the latter value is quite reasonalbe. However, in the present experiment $w \approx 0.1c_s$ and $\Delta(\omega/k) \approx 0.2c_s$; the condition (9) is not satisfied. Therefore the validity of eqs.(7') and (8') should be examined. The most straightforward way is to compare the heating distances, $\ell_{//}$ and $\ell_{\perp}$, predicted by eq.(7') and by eq.(8') with the experimental values, $\ell_{//} = 30\lambda_D$ and $\ell_{\perp} = 360\lambda_D$. From eq.(7') we obtain $\ell_{//} = 70\lambda_D$, $\ell_{\perp} = 500\lambda_D$, and from eq.(8') $\ell_{//} = 11\lambda_D$, $\ell_{\perp} = 80\lambda_D$. The experimental value lies between the two theoretical values. This fact reflects that the turbulence is in an intermediate state, i.e. $w \approx \Delta(\omega/k)$.

4.1.2 Correlation length of the wave

The above discussions on the deformation of $f(v, \theta)$ do not acount for the observed very short correlation

length of the waves. As a mechanism of destructing the coherence of the waves, a few nonlinear processes such as the nonlinear Landau-damping[12,21-23], the resonant three-wave coupling[21,22] and the turbulence-induced collisions[9,20,21] have been proposed.

We first consider the nonlinear Landau-damping. If two waves, propagating at almost the same angle the beam but in the opposite perpendicular direction, couple each other, they can produce a forced beat oscillation propagating almost at right angle to the beam with a very small phase velocity. The interaction of the beat oscillation with the ions will cause a heavy damping of the waves. On the basis of the collisionless Boltzmann equation for ions, the third order perturbation theory gives the following nonlinear damping rate[23],

$$\left|\frac{k_i}{k}^{NL}\right| \gtrsim -2l\sum_{\vec{k}'} \frac{\left|2(\vec{k}\cdot\vec{k}') - k^2\right|^2}{\left(\frac{4c_s^2}{u^2\cos^2\alpha} - 1\right)\cdot\cos\alpha} \left(\frac{c_s}{\vec{k}\vec{u}}\right)^4 c_s^2 \frac{\Delta\vec{k}}{|\Delta\vec{k}|}\cdot\frac{\partial f_0}{\partial\vec{v}}\Big|_{\frac{\Delta\omega}{\Delta\vec{k}}} \cdot \left|\frac{e\phi_{\vec{k}'}}{T_e}\right|^2$$

$$\gtrsim 2\frac{T_e}{T_i} \frac{(1 - 2\cos 2\alpha)^2}{\left(\frac{4c_s^2}{u^2\cos^2\alpha} - 1\right)\cos^5\alpha} \left(\frac{c_s}{u}\right)^2 \left(\frac{\delta n}{n_0}\right)^2, \qquad (10)$$

where $\Delta\vec{k} = \vec{k} - \vec{k}'$, $\Delta\omega = \omega_{\vec{k}} - \omega_{\vec{k}'}$, and $\cos\alpha = (\vec{q}\cdot\vec{u})/qu$. The inequality is due to the strong dependence on the value of $\Delta\omega/\Delta k$ of this process. This damping rate corresponds to

the correlation length, i.e. $L_c \sim |1/k_i^{NL}|$. If we use the representative values of the parameters in Fig.9 such as $T_e = 3$ eV, $T_i = 0.2$ eV, $\alpha = 50^\circ$ and $m_i u^2/2 = 4.9$ eV, we obtain

$$\left|\frac{k_i^{NL}}{k}\right| \lesssim 90\left(\frac{\delta n}{n_0}\right)^2. \qquad (10')$$

The experimental value $|k_i^{NL}/k| \gtrsim 3$ requires $n/n_0 \gtrsim 6 \times 10^{-2}$. This value is consistent with the experiment. However, it should be noted that the assumption of free orbit made in the derivation of eq.(10) is not compatible with the diffusion tensor (8'). Therefore another process must be examined if it exists although above nonlinear effect cannot be neglected.

The spatial correlation measurements have shown that both the wavenumber and the angle of propagation increase with frequency (§3·3(c)). This property inhibits the conservation of $\vec{k}$ and ω when we consider resonant three-wave coupling. However, the broadening of resonance due to the turbulence enables the matching of three waves. Following the procedure developed by Tsytovich[21] we obtain the damping rate

$$\frac{k_i^{NL}}{k} \gtrsim \frac{1}{48\pi}(kL_c)\left(\frac{kc_s}{\omega_{\vec{k}}}\right)^2\left(\frac{\delta n}{n_0}\right)^2 \gtrsim \frac{1}{4}\left(\frac{\delta n}{n_0}\right)^2. \qquad (11)$$

This damping rate, however, is negligibly small compared to the one estimated from (10').

Finally, we exmine the effective collisions arising from the turbulent electric field. Dupree and Tsytovich have proposed that the oscillating part of the velocity distribution function $f(v, x, \theta)$ obeys a diffusion equation similar to eq.(6). This can be interpreted in terms of a turbulent collision, whose frequency ν_{turb} is related to the diffusion tensor

$$\nu_{turb} = (k^2|D|)^{1/3}. \tag{12}$$

Using the expression (8'), we obtain

$$\nu_{turb} = 0.9\ kc_s(\frac{\delta n}{n_0})^{1/2}. \tag{12'}$$

From this relation the damping rate $|k_i^{NL}|$ is estimated to be

$$|\frac{k_i^{NL}}{k}| = 1.8\ \frac{c_s}{u\cdot\cos\alpha}\ (\frac{\delta n}{n_0})^{1/2}. \tag{12''}$$

if $\delta n/n_0 = 5.8 \times 10^{-2}$, we obtain $|k_i^{NL}/k| = 1/3$.

As is shown in Table I, the above examined nonlinear processes can be classified into two groups, Free Orbit and Modified Orbit, depending on whether the orbit modification is essential or not. The expressions (7') and (10) are based on the assumption of free orbit, while (8') and (12)

are of modified orbit. Since $1/\Delta(\omega/k) \gtrsim 1$, it is difficult to decide which process is dominant; the modification of the ion orbit affects the evolution of the turbulence as much as the effects predicted on the basis of free orbit.

4.2 Heating of background ions

The heating of the electrons are not observed. In contrast to the electron-current driven ion-acoustic instability, the i-i instability is caused only by the ion current, which makes the electron dynamics less essential for the evolution of a turbulence. Therefore, the heating of the electrons is neglected in the following discussion.

Although no heating of the background ions is observed, a careful consideration is necessary, because there is no reason that they are not heated by the turbulence. Let us consider the data shown in Fig.9 as an example. Around the position x = 3 cm where $\delta n/n_0$ and $T_{b//}$ [$\equiv T_b(\theta = 0^\circ)$] exhibit exponential growth, the rate equations for the kinetic energy of the beam ions, for their thermal energy and for the wave energy are

$$n_b \frac{d}{dx} \left(\frac{1}{2} m_i u^2\right) \gtrsim -1.4 \times 10^{-3} \frac{n_p}{\lambda_D}$$

(eV/cm^3/Debye length), (13a)

$$n_b \frac{d}{dx} - (2T_{b\perp} + T_{b//}) \gtrsim 0.36 \times 10^{-3} \frac{n_p}{\lambda_D}, \quad (13b)$$

$$\frac{d}{dx}\left[\frac{1}{2} n_p \left(\frac{\delta n}{n_0}\right)^2 T_e\right] \approx 0.3 \times 10^{-3} \frac{n_p}{\lambda_D} . \qquad (13c)$$

These equations claim the existence of an energy absorber, which must be the background ions. If we assume the heating rate of the background ions is equal to that of the beam ions, the enrgy flow to them is

$$n_i \cdot 3 \frac{dT_i}{dx} \approx n_i \cdot 3 \frac{dT_b}{dx} \approx 1.3 \times 10^{-3} \frac{n_p}{\lambda_D} . \qquad (13d)$$

This value is somewhat too large for (13a) to balance with the sum of (13b), (13c) and (13d). The discrepancy is due to the overestimation in (13d); the background ions at x = 3 cm, for example, do not experience the turbulence in other places. The energy fed to the background ions is carried away through the collisions with the low temperature neutral argon atoms. The mean-free-path for the charge exchange process is sufficiently short to take away the energy from the background ions.

4.3 Comments on the formation of turbulent electrostatic shock

In closing this section we consider the posibility of the formation of a turbulent electrostatic shock[24]. This type of shock is of interest because it may have a Mach number M larger than $M_c = 1.6$[25]. A few years ago, McKee[26] discussed this problem on the basis of the one=

dimensional numerical simulation; he concluded that no shock occurs when $M \gtrsim 6$. We comment on this problem from the view point of ion-heating. According to ref.24, one of the conservation equations to be satisfied when the shock is formed is

$$M^2 = \left(\frac{u}{c_s}\right)^2 = 16 \left(\frac{T_{if}}{T_e}\right) \frac{1}{\left(3 - \frac{2T_i}{m_i u^2}\right)\left(1 + 10 \frac{T_i}{m_i u^2}\right)}$$

$$\gtrsim 16 \frac{T_{if}}{T_e} . \qquad (14)$$

Our experiments have confirmed that the final temperature T_{if} does not exceed $0.2\ T_e$. Therefore, M cannot exceed 1.8. The experimental investigation of the electrostatic ion-acoustic shock wave in the Double Plasma Device has shown that a laminar shock with $M \leq 1.5$ is formed when an ion beam is injected into a plasma[13]. It is known also that a quasi-stationary jump in the electrostatic potential is required for the formation of the electrostatic shock[13]. This jump is not taken into account in the theory of the turbulent shock[24,26]. These considerations suggest that the role of the i-i instability for the formation of a high Mach number electrostatic shock wave is not significant.

§5. Conclusion

A strong ion-ion two stream instability was excited by injecting a high density ion beam with a large cross-section into a plasma. The linear stability of the i-i system was experimentally confirmed. The nonlinear stage of the instability was investigated in a three-dimensional way, and the following features of the turbulence were found:

(a) The energy density of the turbulent waves does not exceed $3 \times 10^{-3}\ n_p T_e$.

(b) Turbulent waves propagate at large angles to the beam with extremely short correlation lengths, typically $(2\text{-}3) \cdot \lambda$.

(c) The velocity distribution function is rapidly thermalized in the direction of the propagation of dominant turbulent waves, and the growth rate of the wave is reduced.

(d) The explanation of above features claims the effects of the modification of the ion orbit.

(e) Although the turbulence heats the ions rapidly, the final ion temperature does not exceed $0.2\ T_e$.

(f) The dissipation resulting from i-i instability is responsible for the formation of an electrostatic shock wave only when the Mach number is smaller than 1.8.

Acknowledgement

The authors thank Drs. A. Hasegawa, A. Hirose, K. Mima, K. Saeki and S. Watanabe for their valuable discussions. One of the authors (Y. K) indebted to Professor H. Tanaca for his support.

References

1) B. B. Kadomtsev: Plasma Turbulence (Academic Press, London and New York, 1965).

2) T. E. Stringer: Plasma Physics 6 (1964) 267.

3) V. D. Shapiro: Sov. Phys. JETP 17 (1963) 416.

4) R. J. Briggs: Electron-stream Interaction with Plasmas (The M.I.T. Press, Cambridge, Massachusetts, 1964).

5) B. D. Fried and A. Y. Wong: Phys. Fluids 9 (1966) 1084.

6) A. G. Borisenko and G. S. Kirichenko: Sov. Phys. JETP 33 (1971) 207.

7) D. R. Baker: Phys. Rev. Lett. 28 (1972) 1189.

8) D. R. Baker: Phys. Fluids 16 (1973) 1730.

9) R. J. Taylor and F. V. Coronitti: Phys. Lett. 29 (1972) 34.

10) R. J. Taylor, K. R. MacKenzie and H. Ikezi: Rev. Sci. Instr. 43 (1972) 1675.

11) H. Ikezi, Y. Kiwamoto, K. Nishikawa and K. Mima: Phys. Fluids 15 (1972) 1605.

12) H. Ikezi, Y. Kiwamoto: Phys. Rev. Lett. 27 (1971) 718.

13) H. Ikezi, T. Kamimura, M. Kako and K. E. Lonngren: to be published in Phys. Fluids.

14) P. Mahadevan and G. D. Magnuson: Phys. Rev. 171 (1968) 103.

15) D. W. Forslund and C. R. Shonk: Phys. Rev. Lett. 25 (1970) 281.

16) R. L. Morse and C. W. Nielson: Phys. Rev. Lett. 23 (1969) 1087.

17) K. V. Roberts and H. L. Berk: Phys. Rev. Lett. 19 (1967) 297.

18) E. A. Drummond and D. Pines: Nuclear Fusion Suppl. Pt.3 (1962) 1049.

19) A. A. Vedenov, E. P. Velikhov and R. Z. Sagdeev: Nuclear Fusion Suppl. Pt.2 (1962) 465.

20) T. H. Dupree: Phys. Fluids 9 (1966) 1773.

21) V. N. Tsytovich: An Introduction to the Theory of Plasma Turbulence (Pergamon Press, Oxford, 1972).

22) R. Z. Sagdeev and A. A. Galeev: Nonlinear Plasma Theory (W. A. Benjamin, Inc., New York and Amsterdam, 1969).

23) K. Nishikawa: J. Phys. Soc. Japan 29 (1970) 449.

24) D. A. Tidman: Phys. Fluids 10 (1967) 547.

25) R. Z. Sagdeev: Reviews of Plasma Physics ed. by M. A. Leontovich (Consultants Bureau Enterprises, New York, 1966) Vol.4, 23-92.

26) C. F. McKee: Phys. Rev. Lett. 24 (1970) 990.

Figure Captions

Fig.1. Schematic diagram of the experimental device and the potential distribution of the plasma.

Fig.2. Test-wave propagation in the ion beam-plasma system. T_e = 1.9 eV, n_b/n_p = 0.5, and λ_D = 0.05 cm. Exciting voltage V_{ex} = 0.1 V.

Fig.3. Dispersion relation of the ion beam-plasma system. Dots are obtained from the test-wave propagation in a plasma with T_e/T_i = 20 and n_b/n_p = 0.2. Circles denote the phase velocities of the waves shown in Fig.2, and the triangle indicates the growth-rate of the slow wave. Solid lines indicates the phase velocities calculated from eq.(1); dotted line indicates the growth rate of the slow beam mode.

Fig.4. Marginal stability condition. The beam density fraction n_b/n_p = 0.5. Theoretical values are obtained by assuming Maxwellian distribution (dotted line) and Lorentzian distribution (solid lines).

Fig.5. Evolution of electron density perturbation $\delta n/n_0$ (r.m.s.). (a) as a function of $m_i u^2/2$ (eV) with distance x(cm) as a parameter, (b) as a function of distance x with beam kinetic energy $m_i u^2/2$ as a parameter. In the case of (a), n_b/n_p = 0.3 for $m_i u^2/2 \leq 2$ eV and $n_b n_p = 0.3 \cdot (4/m_i u^2)^{1/2}$ for

$m_i u^2/2 \geq 2$ eV.

Fig.6. The spectra of turbulent noise. (a) $T_e = 1.5$ eV, $n_b/n_p = 0.5$, $\lambda_D = 0.032$ cm, (b) $T_e = 1.5$ eV, $n_b/n_p = 0.4$, $\lambda_D = 0.033$ cm. The band-width of the analyzer $\Delta f = 3$ kHz.

Fig.7. Spatial correlations of turbulent waves along the ion beam ($\parallel$, 2.5 cm $\leq x \leq$ 7.5 cm) and transverse to it ($\perp$, 0 cm $\leq y \leq$ 5 cm) when $u/c_s = 2.9$ (a) and when $u/c_s = 1.0$ (b). $T_e = 2.5$ eV and $n_b/n_p = 0.3$.

Fig.8. Direction of the propagation of turbulent waves vs. beam velocity u/c_s. $n_b/n_p = 0.3$ and 2 eV $\leq T_e \leq 3$ eV.

Fig.9. Velocity distribution of ions $f(v, \theta)$. $T_e = 3$ eV, $n_b/n_p = 0.2$ and $\lambda_D = 0.033$ cm.

Fig.10. Water bag approximation of $f(v, \theta)$.
(a) Initial distribution without shielding ions.
(b) Distribution when the instability is stabilized.

Table I. Comparison of nonlinear processes

	Free Orbit		Modified Orbit		Experiment
	Diffusion(7')	M.L.D.(10)	Diffusion(8')	Turb. Coll.(12)	
$\frac{\delta n}{n_0}$ Stability(5) $L_c = 3\lambda$	0.25	$> 6 \times 10^{-2}$	2.3×10^{-2}	5.8×10^{-2}	6×10^{-2}
$(l_\parallel)_{min.}$	$70\lambda_D$		$11\lambda_D$		$30\lambda_D$
$(l_\perp)_{min.}$	$500\lambda_D$		$80\lambda_D$		$360\lambda_D$
$\frac{w}{\Delta(\frac{\omega}{k})}$	$<< 1$		$>> 1$		0.5

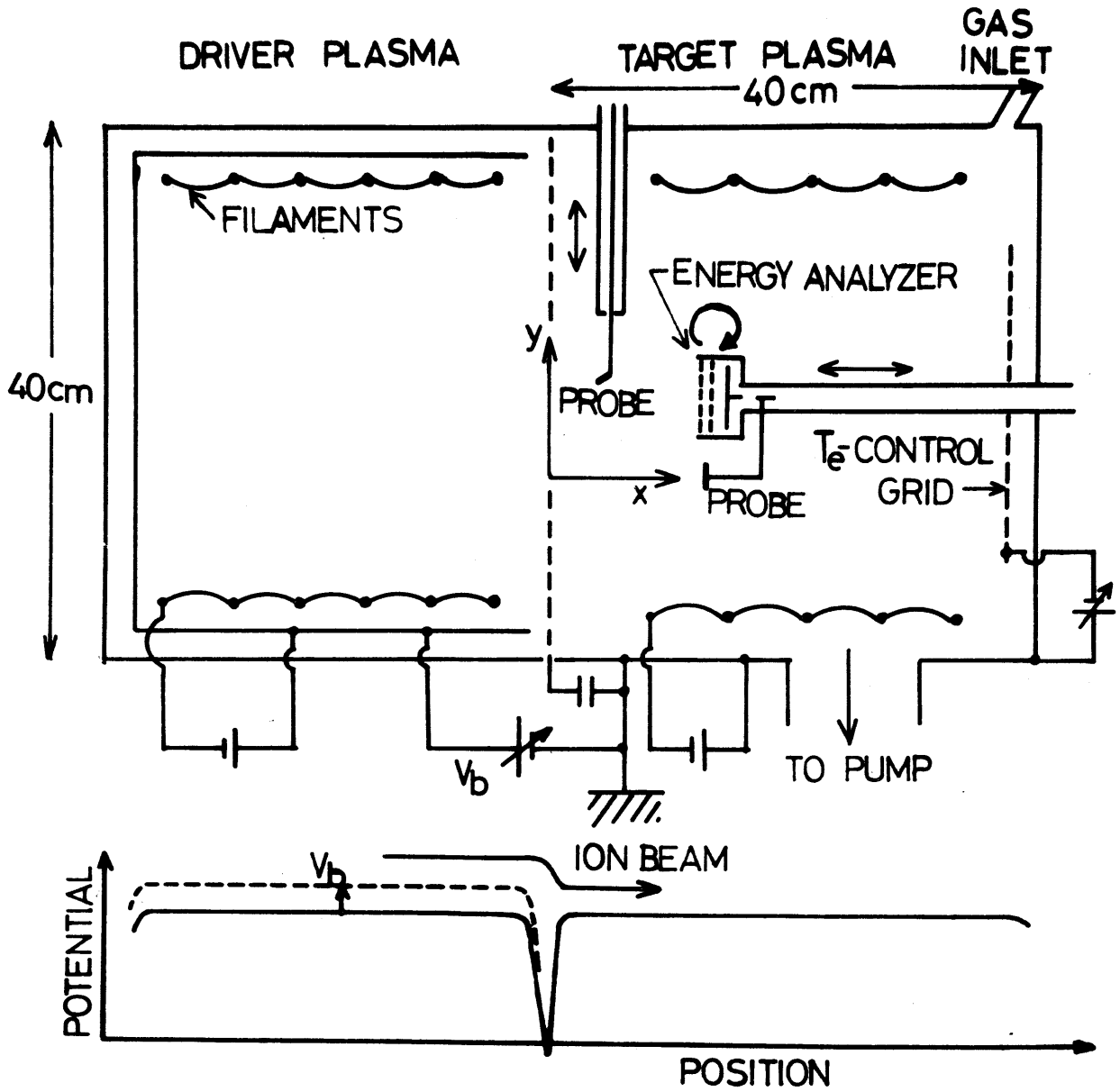
DRIVER PLASMA
TARGET PLASMA
GAS INLET
40cm
FILAMENTS
ENERGY ANALYZER
40cm
y
PROBE
x
PROBE
T_e-CONTROL GRID
V_b
TO PUMP
ION BEAM
V_b
POTENTIAL
POSITION

Fig. 1.

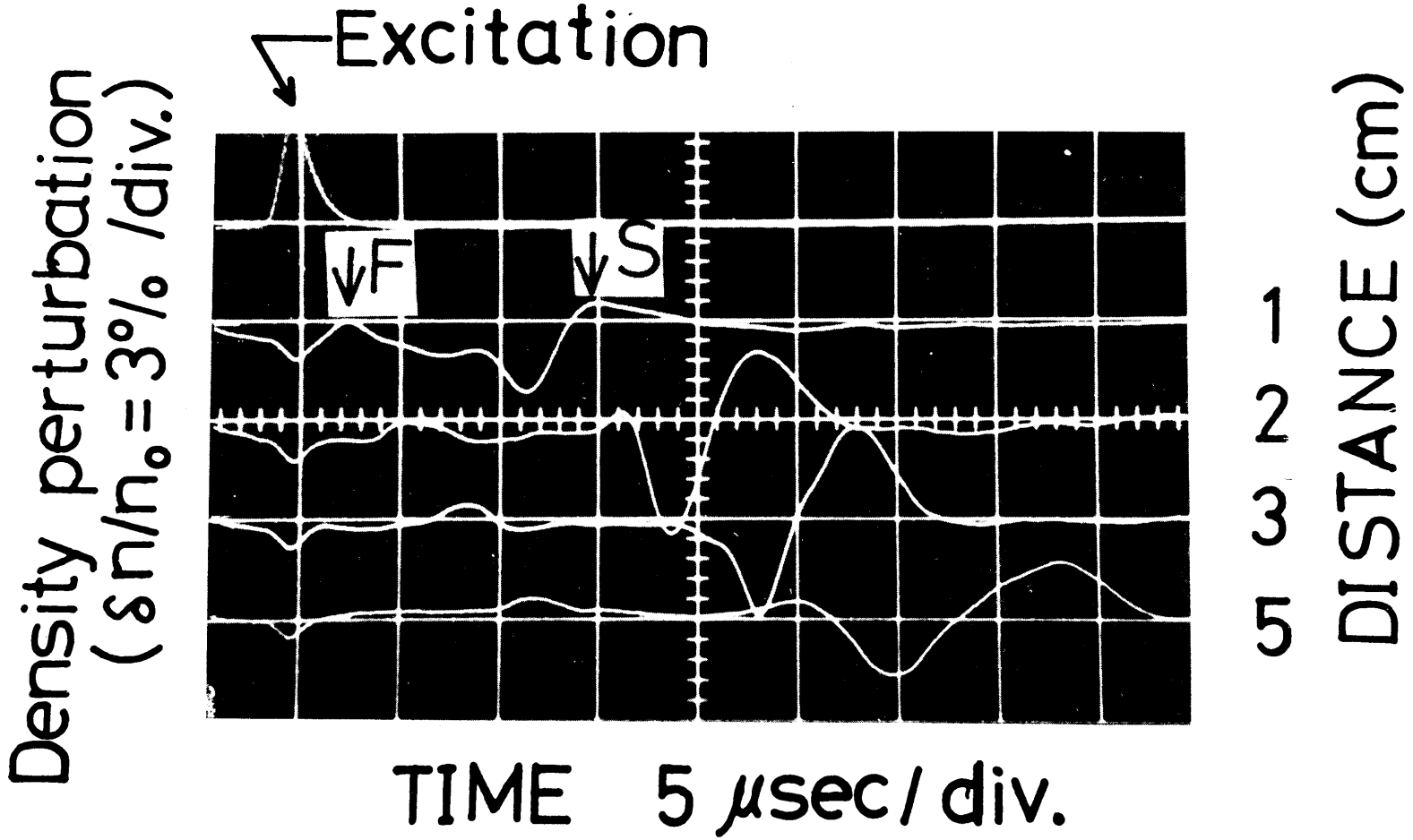
Excitation
F
S
Density perturbation
(δn/n₀= 3% /div.)
1
2
3
5
DISTANCE (cm)
TIME 5 μsec/ div.

Fig. 2.

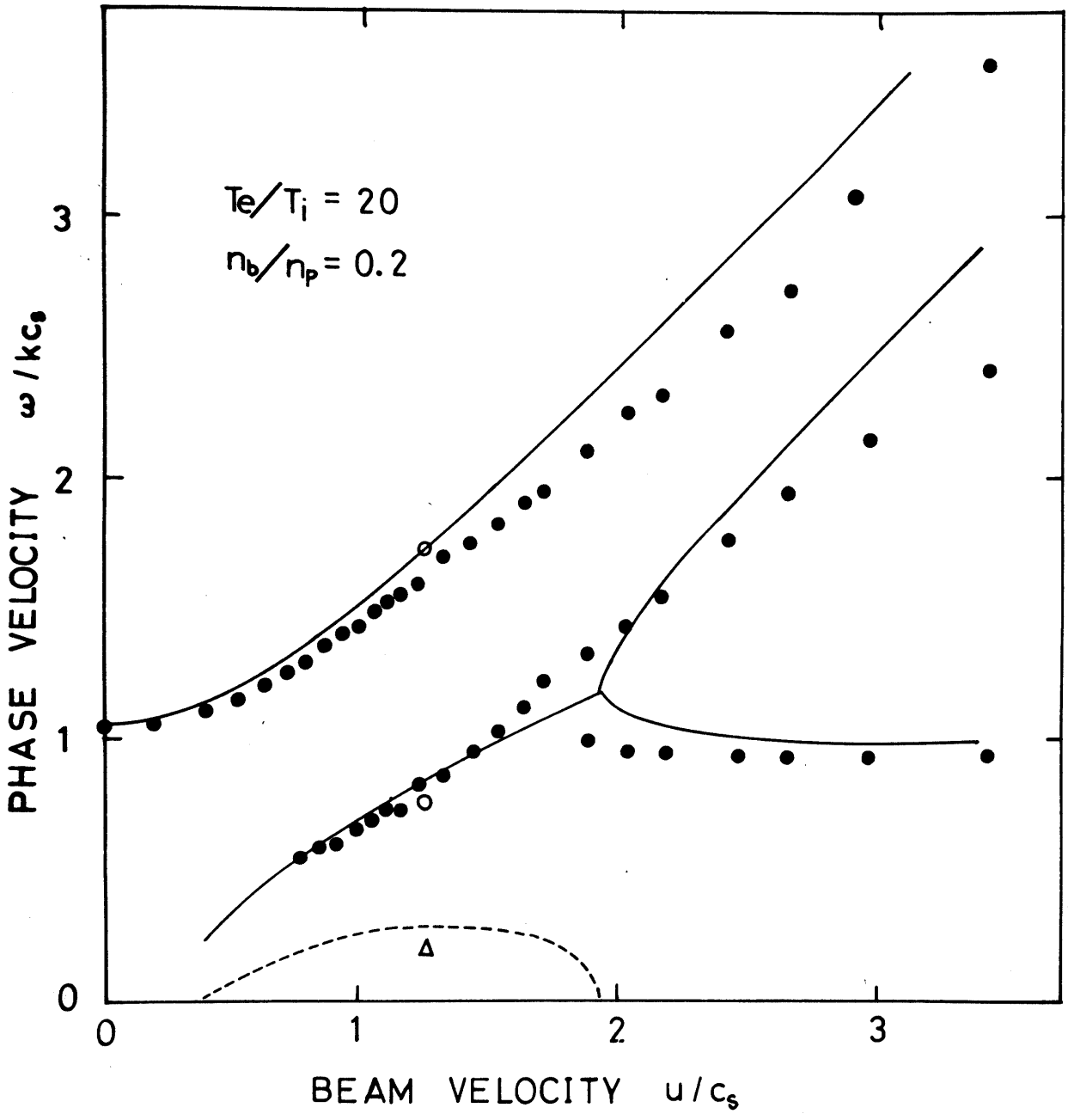

Fig. 3.

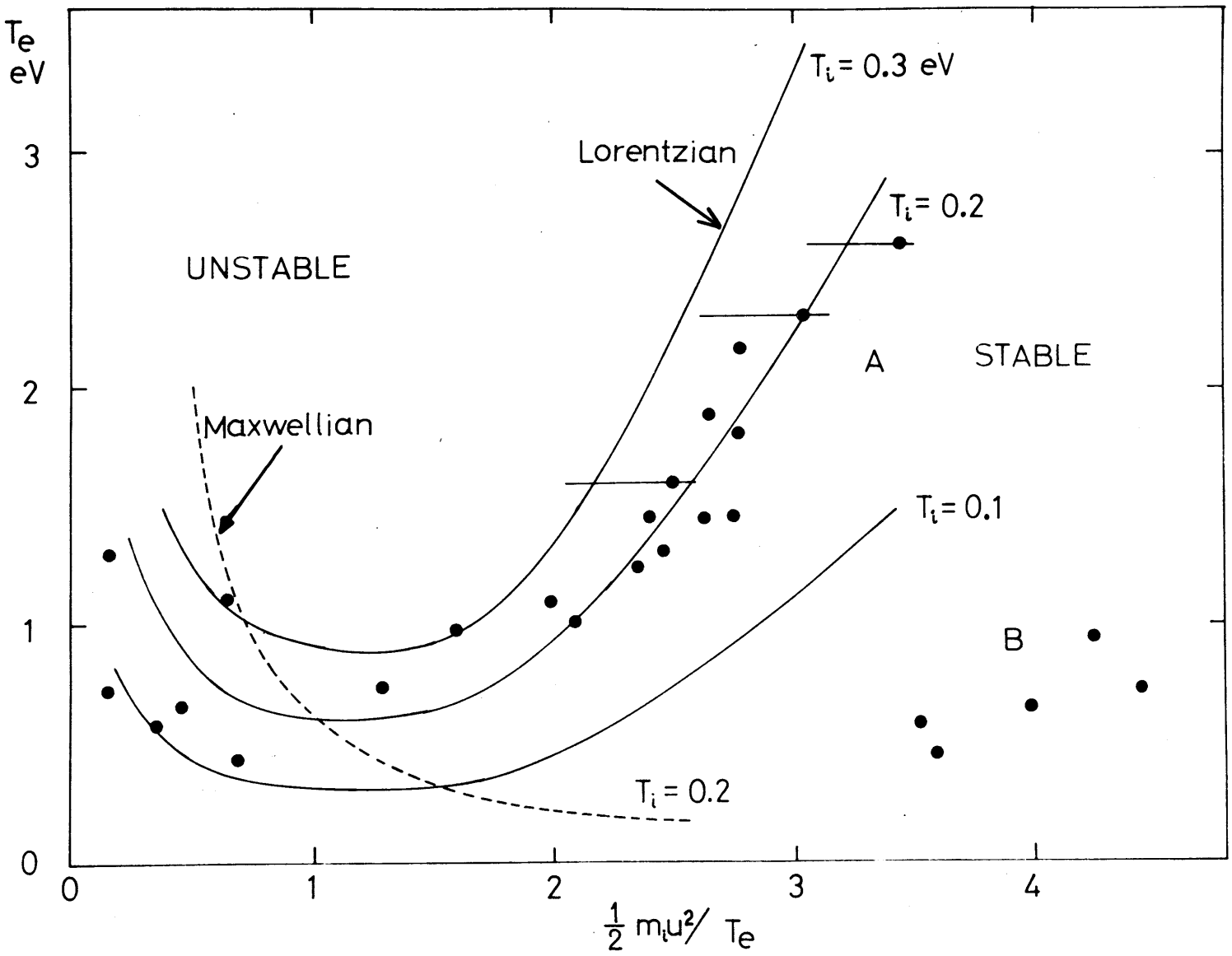
T_e eV
3
2
1
0
0
1
2
3
4
$\frac{1}{2} m_i u^2 / T_e$
T_i = 0.3 eV
Lorentzian
T_i = 0.2
UNSTABLE
A
STABLE
Maxwellian
T_i = 0.1
B
T_i = 0.2

Fig. 4.

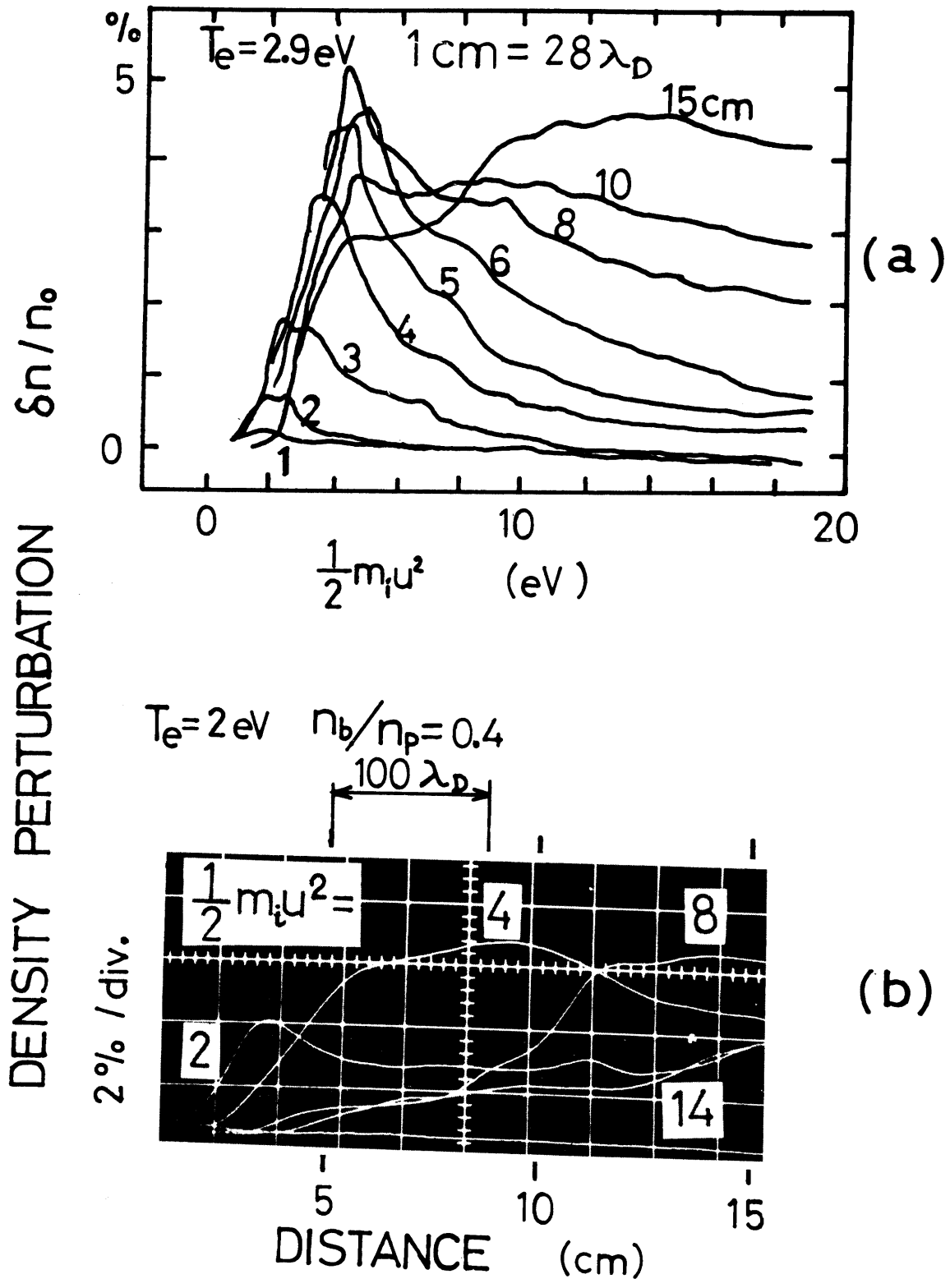
%
5
0
T_e=2.9eV 1cm = 28λ_D
15cm
10
8
6
5
4
3
2
1
0
10
20
$\frac{1}{2}m_iu^2$ (eV)
(a)
DENSITY PERTURBATION $\delta n/n_o$
T_e= 2 eV n_b/n_p= 0.4
100λ_D
$\frac{1}{2}m_iu^2$=
4
8
2
14
2% /div.
5
10
15
DISTANCE (cm)
(b)

Fig. 5.

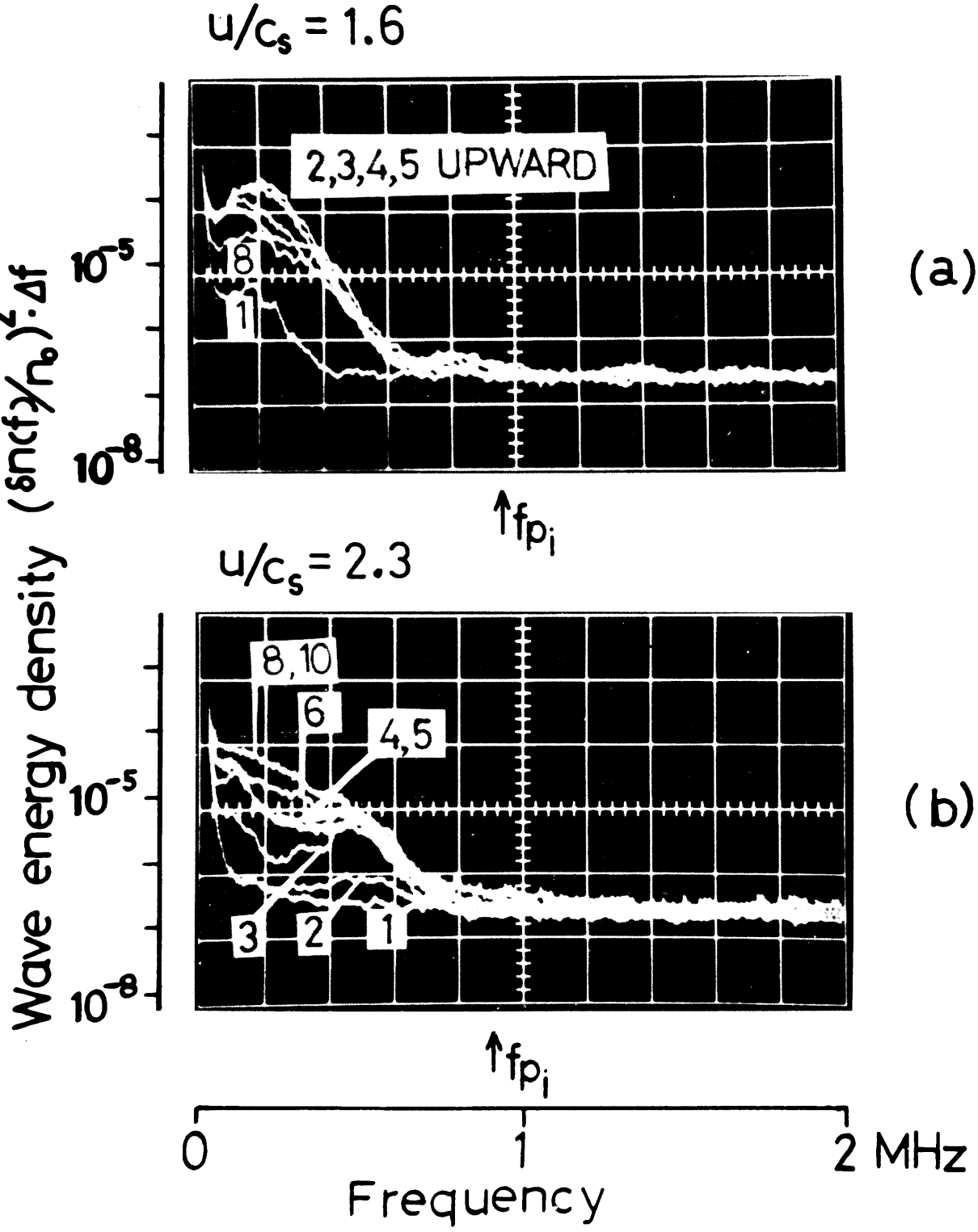
u/cs = 1.6
2,3,4,5 UPWARD
8
1
10-5
10-8
↑fpi
(a)
u/cs = 2.3
8,10
6
4,5
3
2
1
10-5
10-8
↑fpi
(b)
Wave energy density (δn(f)/n0)2·Δf
0
1
2 MHz
Frequency

Fig. 6.

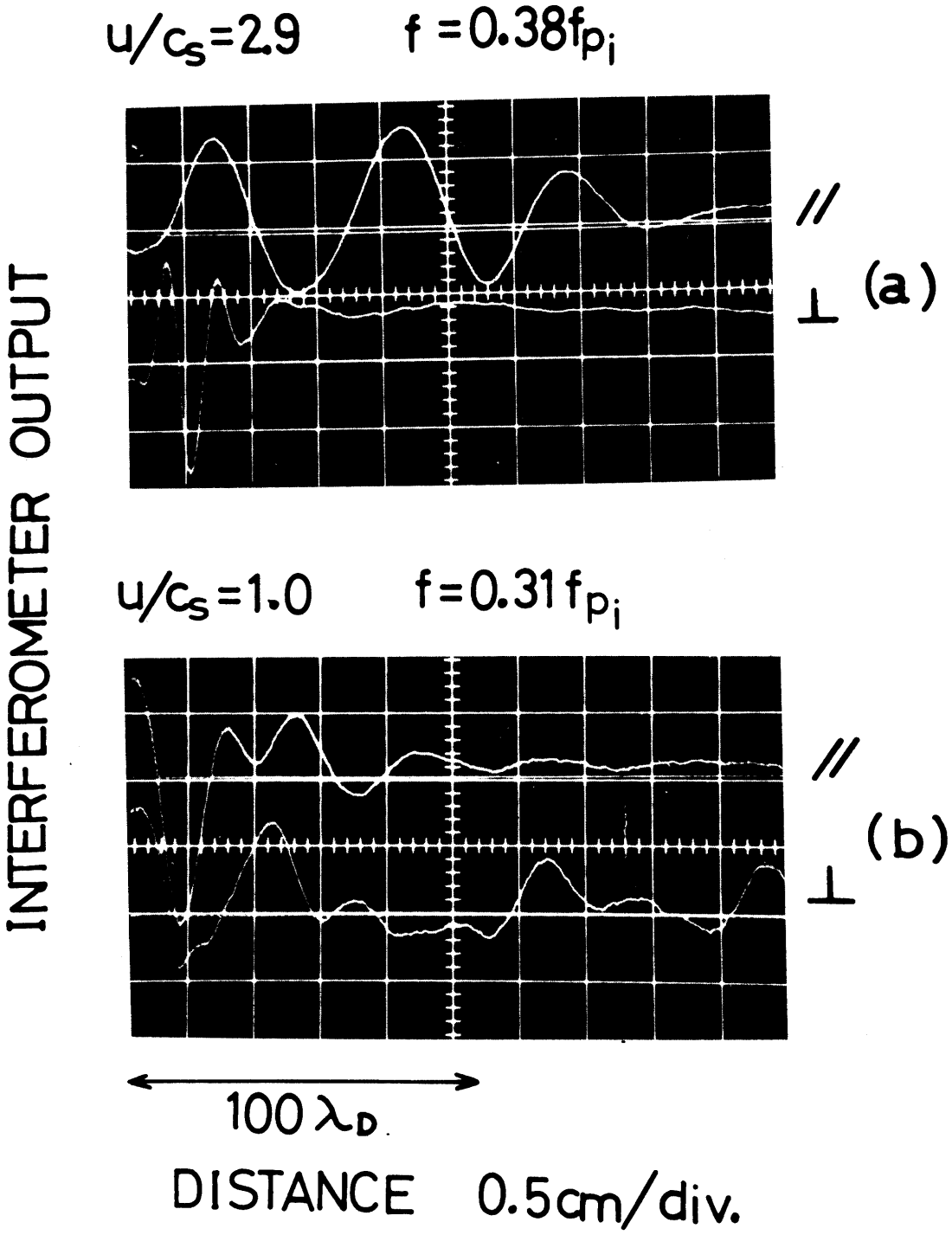
u/cs=2.9
f=0.38fpi
//
⊥
(a)
INTERFEROMETER OUTPUT
u/cs=1.0
f=0.31fpi
//
⊥
(b)
100λD
DISTANCE 0.5cm/div.

Fig. 7.

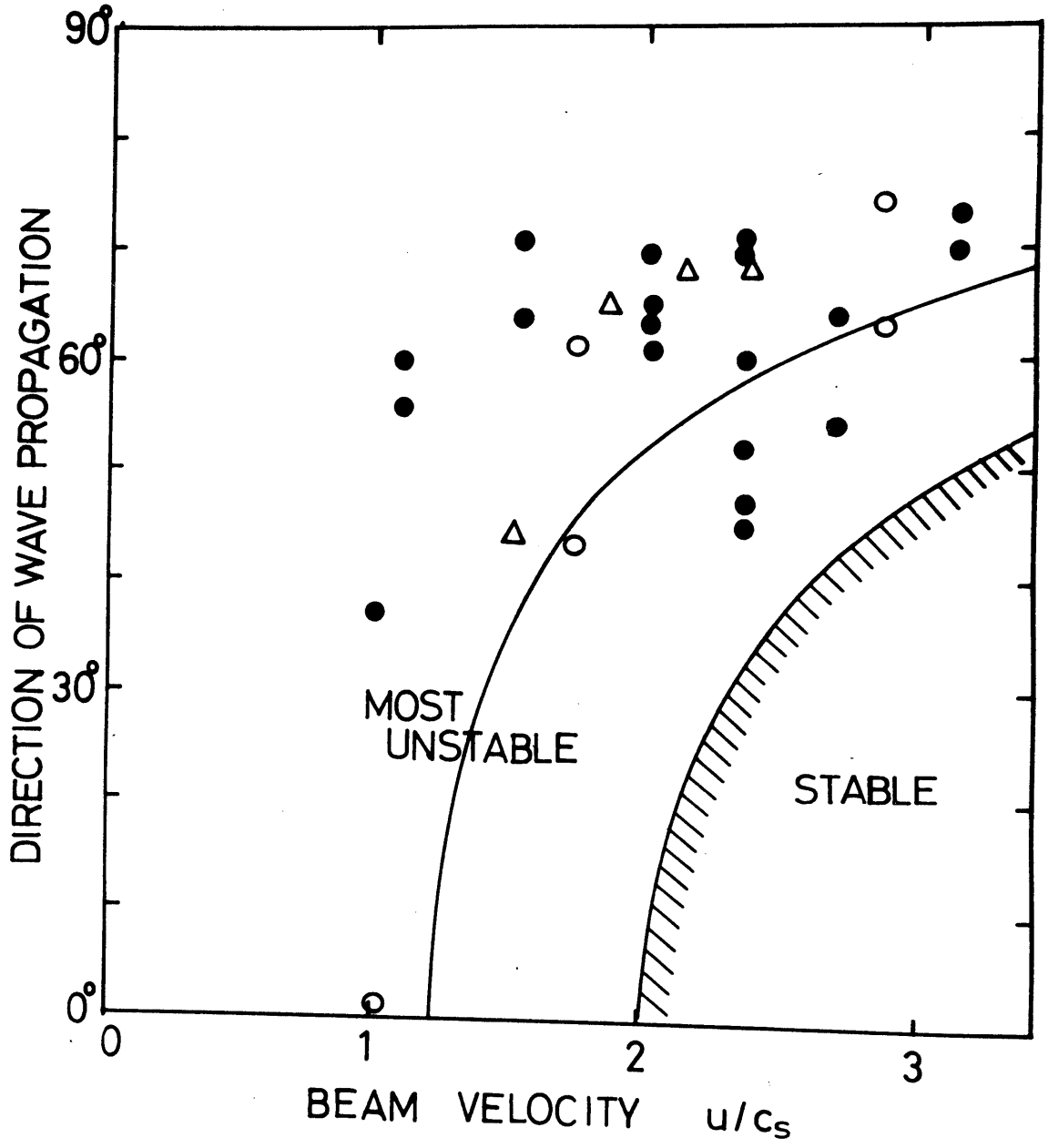
90°
60°
30°
0°
DIRECTION OF WAVE PROPAGATION
MOST
UNSTABLE
STABLE
0
1
2
3
BEAM VELOCITY u/cs

Fig. 8.

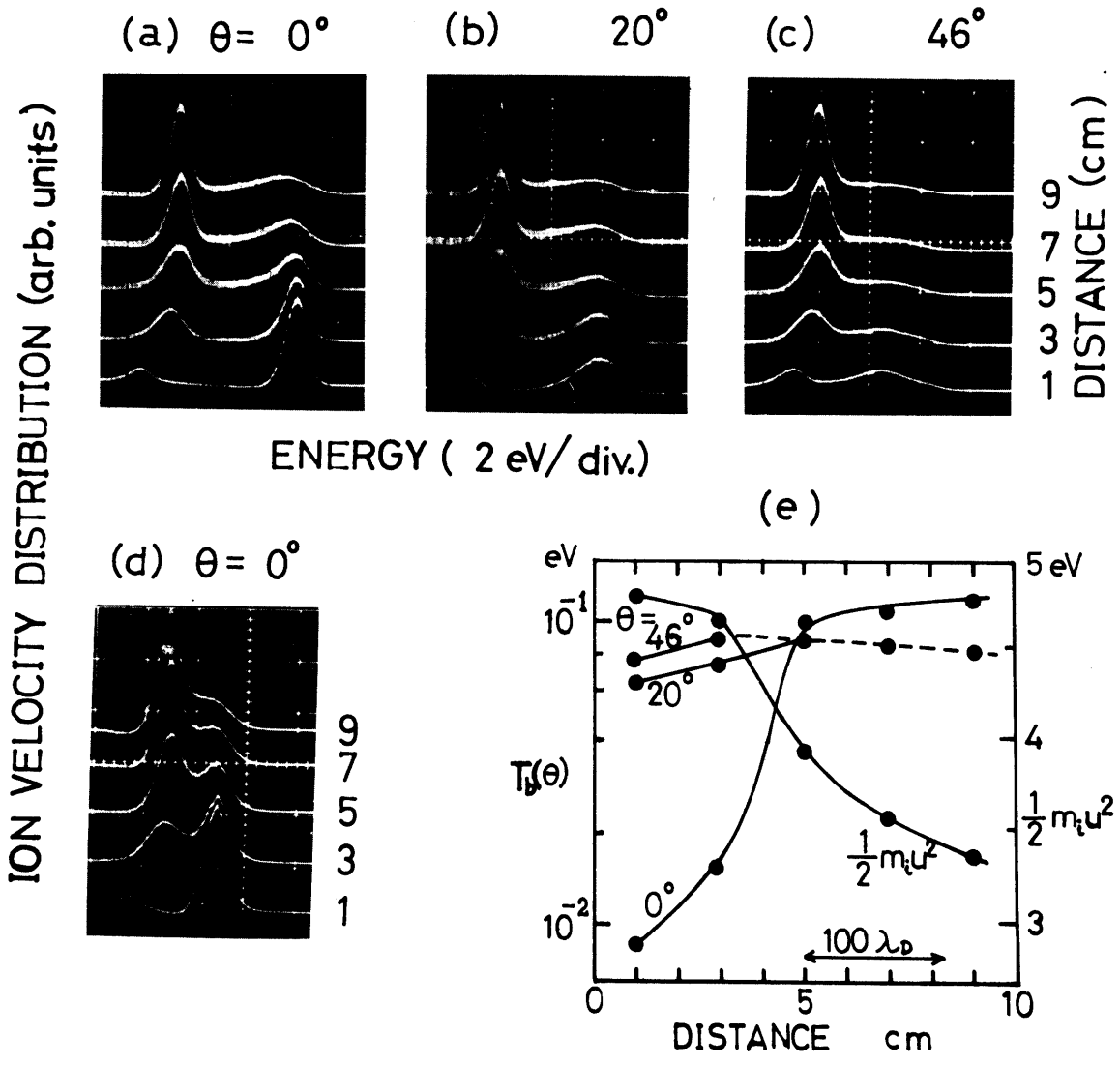
(a) θ= 0°
(b) 20°
(c) 46°
ION VELOCITY DISTRIBUTION (arb. units)
DISTANCE (cm)
9
7
5
3
1
ENERGY (2 eV/ div.)
(d) θ= 0°
(e)
eV
5 eV
10^{-1}
θ = 46°
20°
$T_i(\theta)$
4
$\frac{1}{2}m_iu^2$
$\frac{1}{2}m_iu^2$
10^{-2}
0°
3
100 λ_D
0
5
10
DISTANCE cm

Fig. 9.

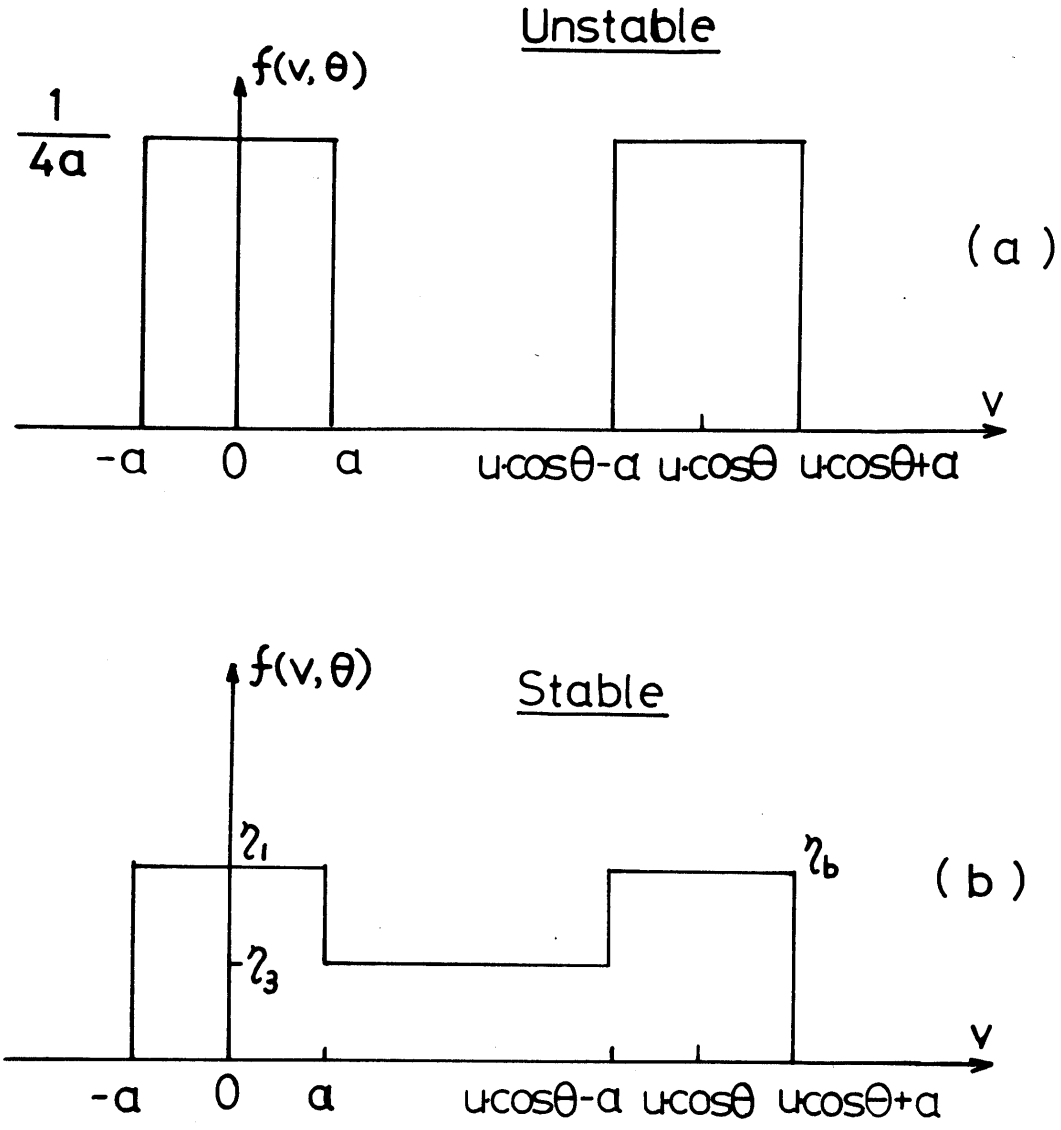
Unstable
f(v, θ)
1/4a
(a)
v
-a
0
a
u·cosθ-a
u·cosθ
u·cosθ+a
f(v, θ)
Stable
η1
η3
ηb
(b)
v
-a
0
a
u·cosθ-a
u·cosθ
u·cosθ+a

Fig. 10.